HHS Public Access

Author manuscript

Biomaterials. Author manuscript; available in PMC 2019 July 01.

Published in final edited form as:

Biomaterials. 2018 July ; 169: 61–71. doi:10.1016/j.biomaterials.2018.03.049.

Decellularized materials derived from TSP2-KO mice promote enhanced neovascularization and integration in diabetic wounds

Aaron H. Morris[1,3], **Danielle K. Stamer**[1], **Britta Kunkemoeller**[2,3], **Julie Chang**[1], **Hao Xing**[1,3], and **Themis R. Kyriakides**[1,2,3]

[1]Department of Biomedical Engineering, Yale University; New Haven CT 06511

[2]Department of Pathology, Yale University; New Haven CT 06511

[3]Vascular Biology and Therapeutics Program, Yale University; New Haven CT 06511

Abstract

Decellularized biologic scaffolds are gaining popularity over synthetic biomaterials as naturally derived materials capable of promoting improved healing. Nevertheless, the most widely used biologic material – acellular dermal matrix (ADM) – exhibits slow repopulation and remodeling, which prevents integration. Additionally, engineering control of these materials is limited because they require a natural source for their production. In the current report, we demonstrate the feasibility of using genetically engineered animals to create decellularized biologic scaffolds with favorable extracellular matrix (ECM) properties. Specifically, we utilized skin from thrombospondin (TSP)-2 KO mice to derive various decellularized products. Scanning electron microscopy and mechanical testing showed that TSP-2 KO ADM exhibited an altered structure and a reduction in elastic modulus and ultimate tensile strength, respectively. When a powdered form of KO ADM was implanted subcutaneously, it was able to promote enhanced vascularization over WT. Additionally, when implanted subcutaneously, intact slabs of KO ADM were populated by higher number of host cells when compared to WT. *In vitro* studies confirmed the promigratory properties of KO ADM. Specifically, degradation products released by pepsin digestion of KO ADM induced greater cell migration than WT. Moreover, cell-derived ECM from TSP-2 null fibroblasts was more permissive to fibroblast migration. Finally, ADMs were implanted in a diabetic wound model to examine their ability to accelerate wound healing. KO ADM exhibited enhanced remodeling and vascular maturation, indicative of efficient integration. Overall, we demonstrate that genetic manipulation enables engineered ECM-based materials with increased regenerative potential.

Keywords

decellularized; ECM (extracellular matrix); wound healing; Regenerative medicine; tissue engineering; genetically modified matrix

*Corresponding author. 10 Amistad St. Room 301C, New Haven, CT 06519, United States. themis.kyriakides@yale.edu.

Introduction

Regenerative medicine is the rapidly growing field of interventions to reconstruct damaged tissues and implement functional repair after injury, generally using one or a combination of cell therapy, scaffold mediated therapies, or drugs [1]. Regenerative medicine has embraced decellularized materials as a class of biomaterials that present distinct advantages over synthetic materials [2,3]. These benefits include native extracellular matrix (ECM) structure, retention of matrix bound growth factors and other bioactive components, well-tolerated degradation products, and a favorable host response. Acellular dermal matrices (ADMs) are the most popular decellularized materials in the clinic with millions of grafts implanted in patients. Nevertheless, ADMs demonstrate slow repopulation, remodeling, and integration due to their dense ultrastructure [1]. The limitations of these materials are evident in the fact that numerous complications have been reported in patients treated with ADM including wound dehiscence, skin necrosis, and infection, with complication rates as high as 38.7% [4,5]. Delayed remodeling and integration are major limitations of these materials, because they contribute to reconstructive failure [6]. Improved cell repopulation and ultimately integration of the ADM with surrounding tissue will likely reduce complications and improve clinical outcomes [7–10].

Furthermore, engineering control of decellularized materials remains difficult because they are derived from natural sources (either animal tissues or cells *in vitro*) [5,10–13]. Attempts to impart engineering control to decellularized extracellular matrices largely rely on top-down approaches. A growing body of work has examined comminuting the materials into a powder or solubilizing it into a gel [14–29]. These are popular approaches to create tissue fillers from decellularized matrices. Additionally, various studies have examined perforating the ECM to create larger pores within the decellularized tissue [30–32]. Selective removal of ECM components provides another top-down, albeit different, method of customizing decellularized materials [32–36]. While selective removal of components imparts some control of decellularized matrix properties, addition of exogenous factors to these materials provides another method to tune these materials. A number of components have been added to decellularized materials typically by incubating the materials in these factors including: matricellular proteins, hyaluronic acid (HA), heparin, VEGF, EGF, and bFGF [37–40].

Recent interest in producing tunable extracellular matrix-based materials has suggested genetic manipulation of the source cells as a potential method to impart bottom-up control in engineering cell-derived matrix (CDM) [41–43]. For example, overexpression of growth factors by cells producing matrix on a hydroxyapatite scaffold results in a matrix coating enriched in these factors, demonstrating the feasibility of a bottom-up approach [44]. Nevertheless, whether genetic manipulation can impart tunability to entire materials or to bulk material properties of the ECM such as its architecture or mechanics remains unknown. The question we address in this report is two-fold: i) can harvesting tissues from genetically engineered animals result in decellularized materials with distinct properties, and ii) can we develop ECM that induces enhanced cell repopulation and overall integration with host tissues?

We selected thrombospondin-2 (TSP-2) null mice as a source of genetically modified ECM because these mice exhibit altered matrix structure, mechanics, enhanced angiogenesis, and wound healing [45,46]. Thrombospondin-2 is an anti-angiogenic matricellular protein which regulates ECM assembly and collagen fibrillogenesis and its absence is associated with the production of irregular collagen fibrils and fibers [47]. It is highly expressed during development and after injury during the production and remodeling of ECM[48]. Additionally, cells isolated from these mice produce cell-derived matrix (CDM) with altered structure and thrombogenicity [46,49,50]. Specifically, these studies have shown that alignment of endothelial cells and platelet aggregation are enhanced and compromised, respectively, on TSP2 KO CDM. Decellularizing skin from the knockout (KO) animals produced ADM with altered structure and mechanics that demonstrated enhanced cell presence, remodeling, and integration in both a subcutaneous (SC) implant and chronic wound setting, suggesting improved regeneration and enhanced performance over traditional ADM. This work examines a novel material that may rapidly translate to the clinic due to enhanced performance over traditional ADM and provides proof-of-concept that genetically engineered decellularized tissues can provide distinct functional advantages over WT.

Materials and Methods

Isolation and Decellularization of Murine Skin

All procedures were performed in accordance with the regulations adopted by the National Institutes of Health and approved by the Animal Care and Use Committee of Yale University. Isolation and decellularization of murine skin was conducted as previously described [5]. Briefly, 12-14-week-old mice on a C57BL/6J background were shaved and treated with depilatory cream to remove hair. Skins were subsequently harvested, flash frozen, and stored at −80°C until use. Skins were incubated for 6 hours in 0.25% Trypsin-EDTA (Gibco), followed by washes in ddH20 three times for 15 minutes. Skins were incubated in 70% ethanol for 12 hours and 3% H_2O_2 (Sigma) for 15 minutes, followed by two 15 minute washes in ddH20. Skins were then incubated in 1% Triton X-100 (American Bioanalytical) in 0.26% Tris (American Bioanalytical)/0.69% EDTA (Sigma) for 6 hours and then overnight. Skins were terminally sterilized in 0.1% peracetic acid (Sigma) in 4% ethanol for two hours. Finally, skins were washed in ddH_2O six times for fifteen minutes each. All above steps were performed at room temperature on an orbital shaker. Skins received a final wash in serum-free Dulbecco's Modified Eagle's Medium (DMEM; Gibco) with 1% penicillin/streptomycin (Pen Strep; Gibco) on a rotating shaker at 37°C for 24 hours. Afterward, skins were rinsed with ddH_2O, lyophilized, and stored at −80°C until use. Samples of each skin were fixed, prepared for histological analysis, and then stained with hematoxylin and eosin using standard protocols.

Tensile Testing

Lyophilized skins were cut into dog bone-shaped specimens using a scalpel and laser cut stencil. Samples were then permitted to rehydrate in PBS for at least 5 minutes before testing and were kept hydrated during testing. Tissue thickness of each sample was determined by measuring the thickness at 3 points within the narrow section using a Mitutoyo digital micrometer. Samples were glued to sections of sandpaper at the end of their

length and mounted into grips attached to the 10 N load cell of the Instron 5848. Tissues were pulled until failure at a rate of 3.3 mm/min, (n=3). Engineering stress and strain were calculated from force, distance, and tissue dimensions according to the following equations where σ is engineering stress, F is force, A_0 is initial cross-sectional area, ε is engineering strain, l_f is final length, and l_0 is initial length:

$$\sigma = \frac{F}{A_0}$$

$$\varepsilon = \frac{l_f - l_0}{l_0}$$

Biochemical Analysis

Collagen content was determined using a hydroxyproline assay (QuickZyme) according to manufacturer's instructions (n=7). Sulfated glycosaminoglycan (sGAG) content was determined using the Blyscan sGAG assay (Biocolor). Samples were digested in papain overnight at 65°C overnight before proceeding with protocol according to manufacturer's instructions (n=3). Residual DNA was quantified with a DNeasy Blood & Tissue Kit (Qiagen) according to manufacturer's instructions (n=3).

Denaturation Analysis

To analyze denaturation, a recently published protocol was used [51]. The collagen hybridizing peptide (CHP), GGG-$(GPO)_9$, (O represents hydroxyproline) with an N-terminal FITC tag was synthesized by United Peptide. Prior to lyophilization, constructs were embedded in OCT mounting medium (TissueTek). 8 μm thick sections were cut and mounted on slides. WT and TSP-2 KO construct sections were mounted. Additionally, native WT and heat-denatured native WT skins were mounted as controls. Heat denaturation was accomplished by incubating section for 10 minutes at 95°C. Samples were washed 3× for 5 minutes with PBS before incubation in 30 μM FITC-CHP in PBS for 2 hours at 4° C. Samples were rinsed 3× for 5 minutes in PBS before mounting in Vectashield Mounting Medium (Vector Labs) and imaging. Three 10× images of each sample were quantified in ImageJ to determine the integrated density of the FITC signal. Data were then normalized to a percent of the heat denatured control sample. Three experiments were performed (n=3).

Enzymatic Degradation Kinetics

Enzymatic degradation was performed as an accelerated measure of in vivo degradation. First, constructs were massed and cut into 1×1 cm squares. Type IV collagenase (50 U/mL, Sigma) or pepsin (1 mg/mL, Sigma) in PBS (for collagenase) or 0.01N HCL (for pepsin) was added for a final concentration of 5 mg dry weight skin/mL. Samples were incubated at 37°C. At specified time points, the mixture was centrifuged at 18,000 g for 1 minute. 20 uL samples of the digest solution were collected at each time point and stored at −20°C until analysis. Protein concentration of the releasate was evaluated with the Bradford Assay (BioRad) against a BSA standard curve (n=3).

Cell Culture

Cells were maintained *in vitro* with standard protocols. Briefly, mouse embryonic fibroblast cell line NIH/3T3 (ATCC), primary dermal fibroblasts, and RAW 264.37 (ATCC) cells were maintained in growth medium, DMEM (Gibco) with 10% FBS and 1% pen strep. The mouse preosteoblastic cell line MC3T3-E1 (a generous gift from Dr. Mark Horowitz) was maintained in growth medium, MEMα, with 10% FBS and 1% pen strep. Human umbilical cord vein cells (HUVECs, Yale VBT Core Facility) were maintained in M199 medium (Gibco) supplemented with 20% FBS, 1% pen strep, and 3% endothelial cell growth supplement (ECGS).

ECM Solubilization

To analyze the chemoattractant properties of degradation products of constructs, concentrated solubilized ECM was produced by incubating constructs at 10 mg dry weight per mL fluid in a solution of 1 mg/mL pepsin in 0.01 N HCl (Sigma) for 72 hours in a manner similar to that described previously [52]. Solubilized ECM was then neutralized and buffered with 1/10th the digest volume of NaOH and 1/9th the digest volume of 10× PBS.

To create media containing degradation products, solubilized ECM (degradation products) was added to cold serum-free media (appropriate medium selected based on cells) at a final matrix concentration of 50 μg/mL and stored at −20°C until use. Cells were serum-starved overnight before use. NIH/3T3, MC3T3-E1, and RAW 264.37 cells were starved in serum-free media, and HUVECs were starved in 0.5% FBS. Transwells with 8 μm pores (Corning) were coated with 50 ug/mL collagen I (BD) for 30 minutes at 37°C. Cells were harvested by addition of 0.25% Trypsin/EDTA. A suspension of 50,000 cells was added to each Transwell in 100 μL serum-free media. 600 μL media containing degradation products or pepsin control was added to the bottom of the well, and cells were allowed to migrate for 6 hours at 37°C, before being fixed in 100% methanol and stained with a Diff-Quik kit (EMS). Wells were imaged at 20× and quantified by measuring the number of cells per image (n=3).

Subcutaneous Implantation

All procedures were performed in accordance with the regulations adopted by the National Institutes of Health and approved by the Animal Care and Use Committee of Yale University. Decellularized skin was kindly comminuted by the Christman Lab (UCSD). Constructs were passed through a Wiley mini mill (Thomas Scientific, Swedesboro, NJ) and stored in a desiccator until use. Silicone trays were used for subcutaneous implantation of decellularized skin slabs as well as comminuted decellularized skin because of the difficulty of retrieving powdered matrix after implantation. The trays were fabricated by cutting two 6 mm squares of silicone and punching a 4 mm biopsy punch through one of them. The two squares were then treated with oxygen plasma and allowed to form a permanent bond. After tray fabrication, matrix was loaded into the tray to create a layered silicone matrix product similar to that published previously, [53]. 4 mm intact slabs of decellularized matrix or equivalent in thickness powder were placed in the trays and implanted upright SC so that the ECM was in contact with the dermis.

SC implantations were performed as described previously [5,54,55]. Trays were implanted SC for 2 weeks in 12-14 week old C57BL/6 mice. Each mouse received two implants in its dorsal region, each from a different construct. Implants were excised en bloc and prepared for histological analysis. Sections were stained with hematoxylin and eosin according to standard protocols. Additionally, samples were analyzed by immunohistochemistry with antibodies against CD31 (Dianova) and αSMA (Dako). For quantifying cell invasion into intact slabs, histological sections were imaged in the central region of the implant (10×) and the number of cells per high power field (HPF) was quantified in ImageJ (n=4). For quantifying vascularity around powdered skin, three 40× images were taken per implant and the number and size of CD31+ and SMA+ lumens were quantified in ImageJ (n=6).

In Vitro Migration through Cell-Derived Matrix

To probe mechanisms of enhanced cell presence into intact slabs of TSP-2 null ADM, an *in vitro* assay was used in a similar manner to previous work to compare cell migration through WT and TSP-2 null cell-derived matrix (CDM) [46]. Briefly, primary dermal fibroblasts were isolated from WT or TSP-2 KO mouse skin and 50,000 cells were seeded into the top chamber of a Transwell (Corning). Cells were cultured in the presence of 100 μM ascorbic acid for 7 days before decellularization with 40 mM NH_4OH and 0.5% Triton X-100. Next, 50,000 fibroblasts isolated from either WT or db/db mice (serum starved overnight in 0.5% FBS) in 100 μL serum free media were added onto the CDM in the Transwells. 600 μL media with 10% FBS was added below the Transwells, and cells were allowed to migrate at 37°C for 6 hours before being fixed in 100% methanol and stained with a Diff-Quik kit (EMS). Wells were imaged at 20× and quantified by measuring the number of cells per image (n=5).

In Vivo Wound Healing in Diabetic Animals

All procedures were performed in accordance with the regulations adopted by the National Institutes of Health and approved by the Animal Care and Use Committee of Yale University. Homozygous genetically diabetic 12-week-old, Lep/r—db/db mice (B6.BKS(D)-Leprdb/J, Jackson) were used for wound experiments as previously described, [56,57]. The day before surgery, hair was clipped and depilated (Nair). Animals were anesthetized with isothesia, and two symmetric 6 mm full-thickness circular wounds were created on the dorsa of animals using a biopsy punch (Acupunch). Wounds were covered with the appropriate constructs and sutured into place using Polysorb 4-0 suture (Covidien). The entire area was then covered with Tegaderm (3M). Tegaderm was sutured to the skin to ensure scaffold hydration.

At 10 days or 21 days, animals were euthanized and the wound area was excised together with the surrounding tissues for analysis. Wounds were fixed overnight in Z-Fix (Anatech) and prepared for histological analysis by bisecting the wound. Sections were stained with hematoxylin and eosin and Masson’s Trichrome according to standard protocols. Additionally, samples were analyzed by immunohistochemistry, as described above. For quantifying cellular content of grafts, three 20× images were taken per implant and the number of vimentin+ cells and the number and size of CD31+ and SMA+ lumens were quantified in ImageJ. For analysis of collagen remodeling, paraffin-embedded sections were

analyzed as described previously [51]. Briefly, paraffin was removed by incubation in xylenes, and tissue was rehydrated in an ethanol series. Subsequently, sections were blocked in 5% goat serum for 20 minutes. Sections were stained with the collagen-hybridizing peptide and DAPI overnight at 4°C as described above. Slides were washed three times with PBS and mounted with Vectashield Mounting Medium. For quantification, four 40× images were taken along the edge of the construct to examine collagen remodeling. Images were quantified for integrated intensity using ImageJ.

Scanning Electron Microscopy

To prepare samples for SEM, cross-sections of lyophilized skins were mounted to stubs with carbon tape, sputter-coated with iridium, and viewed via SEM (Hitachi SU-70).

Statistical Analysis

Data are expressed as the mean + the standard error of the mean (SEM). One-way ANOVA with Tukey's Multiple Comparisons test were used for all statistical analysis of data with more than two samples. For experiments where data was collected from only two samples, a two-tailed Student's t-test was used. P-values < 0.05 were considered statistically significant.

Results

Genetic manipulation alters scaffold structure and mechanical properties

The process previously optimized for WT mouse skin was also able to adequately decellularize TSP-2 KO skin, [5]. Decellularization resulted in removal of bulk cellular and nuclear material, which was demonstrated by the lack of nuclear remnants on the hematoxylin and eosin (H&E) stained tissue (Fig. 1 B). SEM demonstrated the expected basket-weave morphology of the dermis of the WT construct, contrasting with the less organized morphology of the TSP-2 KO construct (Fig. 1 A). Consistent with this abnormal morphology of TSP-2 KO samples, mechanical testing showed a right-shifted stress-strain curve with lower peaks at failure, corresponding to reduced elastic modulus and ultimate tensile strength (U.T.S.), respectively (Fig. 1 C–F).

Composition, denaturation, and degradation kinetics of ADM

Collagen content was reduced in the TSP-2 KO construct as compared to WT (Fig. 2 A), but sGAG and residual DNA content did not change with genotype (Fig. 2 B–C). The similar residual DNA content was below the commonly accepted threshold for adequate decellularization of 50 ng dsDNA per mg ECM, indicating that the tissues were equally well decellularized. No difference was found in the total amount of denatured collagen between native skin, WT ADM, or KO ADM, but the heat-denatured control demonstrated significantly more denaturation (Fig. 2 D and Supplemental Fig. 1). Digestion of decellularized constructs in purified enzyme solution indicated that WT and TSP-2 KO ADM have equal susceptibility to both collagenase and pepsin (Fig. 2 E–F). It is important to note that *in vivo* degradation is cell-mediated, and thus enzyme susceptibility is not a perfect predictor of material lifetimes *in vivo*.

TSP-2 KO ADM degradation products promote migration

To test whether degradation products of the TSP-2 KO and WT materials had differential chemoattractant effects on cells, the materials were digested in pepsin to create degradation products which were added to media. This preparation was used as the chemoattractant solution in migration assays.

Transwell culture inserts. Several cell types were selected including NIH/3T3 fibroblasts because they are an important cell type in skin homeostasis and secrete their own ECM, MC3T3-E1 preosteoblasts as another cell type that secretes extensive ECM *in vitro*, and HUVECs and RAW 264.7 cells because of the essential role of vascularization and inflammation in wound healing. Enhanced migration toward TSP-2 KO, but not WT degradation products, was observed for NIH/3T3 fibroblasts and MC3T3-E1 preosteoblastic cells (Fig. 3 A and B). HUVECs and RAW 264.7 cells displayed no chemotaxis toward degradation products (Fig. 3 C and D). Differential effects on different cell types indicate that the chemotactic effects of TSP-2 null ADM degradation products are cell-specific. Furthermore, in preliminary experiments, ADM were used as wound coverings for healthy WT mice, and the TSP-2 KO ADM demonstrated accelerated healing by 7 days post-implantation (Supplemental Fig. 2), suggesting the degradation products translated favorable chemoattractant properties to an *in vivo* setting.

Comminuted ECM

Comminuted (or micronized) ECM is popular for use as a tissue filler (e.g. Cymetra) and has been examined as an occlusive dressing for fingertip injuries [14–17]. To study the influence of genetic manipulations on the host response to comminuted ECM, silicone trays were used to implant decellularized skin that had been comminuted (herein referred to as WT or KO powder), subcutaneously (Fig. 4 A–B). The trays were necessary because retrieving powder after *in vivo* application in the SC space was challenging. After two weeks, trays with the ECM were retrieved. H&E-stained sections containing the powdered ECM demonstrate that regardless of genotype, cells invaded throughout (Fig. 4 B). Immunohistochemical staining for CD31 revealed more blood vessels around the TSP-2 KO powder than there were around the WT (Fig. 4 C,D). The vessels were also larger around the KO powder than the WT (Fig. 4 C, F). Additionally, there were more αSMA-positive blood vessels around the TSP-2 KO powder (Fig. 4 D, G). Together, the CD31 and αSMA stains demonstrated enhanced vascularization and vessel maturation around the TSP-2 KO powder.

Enhanced Cell Migration with TSP-2 null ECM

To examine the host response to ADM, 4 mm slabs of intact decellularized skin were implanted subcutaneously in mice in silicone trays for 14 days. After excision and staining with H&E, it was observed that more cells migrated into TSP-2 KO ECM compared to WT (Fig. 5 A–B). To investigate this mechanism *in vitro*, primary dermal fibroblasts were isolated from WT or TSP-2 KO mice and cultured on Transwells to produce a layer of cell-derived matrix (CDM) (Fig. 5 C). This CDM was decellularized and either primary WT fibroblasts or fibroblasts isolated from the genetically diabetic db/db mouse were seeded on top of the matrix in serum-free media. Serum containing media was added to the bottom of the well, and migration through the matrix quantified. In both cases (WT or db/db

fibroblasts) the TSP-2 null matrix was more permissive to fibroblast migration (Fig. 5 D–E). These data are consistent with previous findings demonstrating that TSP-2 KO matrix is more permissive to endothelial cell migration [46].

Diabetic wound healing with ADM

TSP-2 KO constructs demonstrated characteristics that are functionally distinct from WT including altered structure, degradation products, mechanics, and host response. Enhanced cell invasion into TSP-2 KO ECM could make it a useful material in a regenerative medicine setting where accelerated integration is desirable [7,10,58]. Utility in a compromised wound healing scenario, such as diabetic wound healing, is necessary to fully evaluate the material in a regenerative context. To this end, slabs of ADM were rehydrated in PBS and sutured into full thickness wounds of the genetically diabetic db/db mouse. After 10 days, the TSP-2 KO ADM integrated better with the surrounding tissue, to the point where the border between graft and normal tissue could not be discerned (Fig. 6 C). Analysis of collagen demonstrated that the TSP-2 KO constructs underwent more remodeling at 10 days as compared to the WT (Fig. 6 A–B). At 10 days, more vimentin-positive cells, a marker of cells of a mesenchymal lineage, were present within the TSP-2 KO construct than the WT, but by 21 days there was no longer a difference (Fig. 6 E–F). At both time points (10 and 21 d), there were more αSMA-positive vessels within the TSP-2 KO construct, indicating more vessel maturation (Fig. 6 G–H). There was no difference in CD31 staining at either time point (Fig. 6 D).

Discussion

This work presents a proof of principle that genetic manipulations can serve as a toolbox to impart tunability to ECM-based materials that results in increased functional performance. Although the current report only demonstrates functionally distinct materials from a single gene knockout animal, this work can serve as a foundation from which a number of genetic manipulations may permit tunability in ECM-derived materials. Specifically, we show that genetically engineered materials may demonstrate superior cell repopulation, remodeling, and integration over native ECM. While previous work has demonstrated that ECM coatings can be enriched in particular factors by their upregulation via genetic techniques, this work examines more fundamental aspects of bulk material properties, namely structure and mechanics. Additionally, this work examines whole tissue-derived materials rather than only CDM coatings and details improvements in tissue integration of ADM with genetically engineered source material in the subcutaneous space as well as in a compromised model of wound healing.

We have demonstrated that tissues from a genetically modified mouse can be decellularized with techniques already in use for WT tissues, and that the resulting material exhibits altered structural and thus mechanical properties. Both structure and mechanics are central to the function of any material, and the ability to manipulate these properties is one advantage that synthetic materials currently retain over decellularized ECM. Additionally, although the biomaterial exhibits only subtle biochemical differences, its degradation products have a pronounced chemoattractant effect on specific cell types.

In vivo, subcutaneous implantation experiments demonstrated that TSP-2 KO ADM is more permissive to cell migration. This phenomenon was recapitulated *in vitro* with cell-derived matrix, suggesting a functional change in the manner in which fibroblasts interact with TSP-2 KO ECM as compared to WT. Furthermore, when the ADMs were comminuted into a powdered form, TSP-2 KO was able to promote a significant increase in vessel formation and vascular maturity by 14 days, suggesting it may function as an improved tissue filler over the traditional WT materials.

Moreover, the genetically modified ADM demonstrated accelerated wound healing in a diabetic model of compromised healing. TSP-2 KO constructs exhibited enhanced integration at 10 days, evident in the difficulty of discerning the graft-skin border compared to WT, increased remodeling of the graft, enhanced vimentin+ cell invasion, and increased number of αSMA+ vessels. The findings of increased cell repopulation, ECM remodeling, and integration suggest that these materials may be advantageous in the clinic for the treatment of chronic wounds. Lack of integration with the host tissue is thought to be the largest contributor to high complication rates of decellularized materials, which strengthens this suggestion [6,58]. Furthermore, enhanced cell presence and constructive remodeling within acellular materials lead to improved downstream outcomes in general [7,8,10].

There will be 300 million diabetics worldwide by 2025, and 15-20% of diabetics develop non-healing wounds [59,60]. Thus, materials that can accelerate healing of chronic wounds clearly have the potential to influence a large population. Although these materials are time-consuming and expensive to produce, the expense is likely worth the cost, because as many as 22% of patients with non-healing wounds will require amputation, a procedure with a five-year mortality rate of 50% [60,61]. Therefore, there is a tremendous clinical need for regenerative medicine to speed recovery in diabetic wounds. Current ADMs exhibit slow repopulation and integration with surrounding tissue limiting their use as successful interventions in non-healing diabetic wounds. Accelerated integration of acellular materials could improve their utility in a variety of settings including making them more attractive candidates for use in non-healing wounds.

Genetic engineering has the potential to impart tunability to decellularized ECM-derived materials that is simply not attainable with traditional techniques. Although scale-up for the clinic using murine skin is not feasible, future work could extend the present findings to the creation of materials from a TSP-2 KO large animal model for human use. Additionally, other genetic modifications should be investigated to expand the toolbox. For example, other matricellular proteins such as secreted protein acidic and rich in cysteine (SPARC) that influence ECM assembly could be explored or modulations between simply WT and KO such as interventions to partially inhibit particular proteins could be investigated. Ultimately, this work provides a foundation for using genetically engineered ECM for creation of pro-regenerative materials for the clinic.

Supplementary Material

Refer to Web version on PubMed Central for supplementary material.

Acknowledgments

We would like to thank Blake Thomson for helpful discussions and assistance. This work was funded by National Institutes of Health Grants (GM-072194). This material is based upon work supported by the National Science Foundation Graduate Research Fellowship under Grant No. DGE-1122492 (A.H.M.). Any opinion, findings, and conclusions or recommendations expressed in this material are those of the authors and do not necessarily reflect the views of the National Science Foundation. Use of core facilities was supported by YINQE and NSF MRSEC DMR 1119826.

References

1. Londono R, Badylak SF. Biologic Scaffolds for Regenerative Medicine: Mechanisms of In vivo Remodeling. Ann Biomed Eng. 2014; doi: 10.1007/s10439-014-1103-8
2. Aamodt JM, Grainger DW. Extracellular Matrix-based Biomaterial Scaffolds and the Host Response. Biomaterials. 2016; 86:68–82. DOI: 10.1016/j.biomaterials.2016.02.003 [PubMed: 26890039]
3. Morris AH, Kyriakides TR. Matricellular proteins and biomaterials. Matrix Biol. 2014; doi: 10.1016/j.matbio.2014.03.002
4. Garvey PB, Giordano SA, Baumann DP, Liu J, Butler CE. Long-Term Outcomes after Abdominal Wall Reconstruction with Acellular Dermal Matrix. J Am Coll Surg. 2017; 224:341–350. https://doi.org/10.1016/j.jamcollsurg.2016.11.017. [PubMed: 27993696]
5. Morris AH, Chang J, Kyriakides TR. Inadequate Processing of Decellularized Dermal Matrix Reduces Cell Viability *In Vitro* and Increases Apoptosis and Acute Inflammation. In Vivo, Biores Open Access. 2016; 5:177–187. DOI: 10.1089/biores.2016.0021 [PubMed: 27500014]
6. Bullocks JM. DermACELL: a novel and biocompatible acellular dermal matrix in tissue expander and implant-based breast reconstruction. 2014; :529–538. DOI: 10.1007/s00238-014-0995-8
7. Lopresti, ST., Brown, BN. Host Response to Naturally Derived Biomaterials. In: Badylak, S., editor. Host Response to Biomater. Impact Host Response Biomater Sel. Academic Press; 2015. p. 53-73.
8. Valentin JE, Badylak JS, McCabe GP, Badylak SF. Extracellular matrix bioscaffolds for orthopaedic applications. A comparative histologic study. J Bone Joint Surg Am. 2006; 88:2673–86. DOI: 10.2106/JBJS.E.01008 [PubMed: 17142418]
9. Moyer HR, Hart AM, Yeager J, Losken A. A Histological Comparison of Two Human Acellular Dermal Matrix Products in Prosthetic-Based Breast Reconstruction. Plast Reconstr Surg – Glob Open. 2017; 5:e1576.doi: 10.1097/GOX.0000000000001576 [PubMed: 29632762]
10. Morris AH, Stamer DK, Kyriakides TR. The host response to naturally-derived extracellular matrix biomaterials. Semin Immunol. 2017; :1–20. DOI: 10.1016/j.smim.2017.01.002
11. Luten J, van Nostrum CF, De Smedt SC, Hennink WE. Biodegradable polymers as non-viral carriers for plasmid DNA delivery. J Control Release. 2008; 126:97–110. DOI: 10.1016/j.jconrel.2007.10.028 [PubMed: 18201788]
12. During MJ, Freese A, Sabel BA, Saltzman WM, Deutch A, Roth RH, Langer R. Controlled release of dopamine from a polymeric brain implant: in vivo characterization. Ann Neurol. 1989; 25:351–6. DOI: 10.1002/ana.410250406 [PubMed: 2634975]
13. Mikos AG, Temenoff JS. Formation of highly porous biodegradable scaffolds for tissue engineering. Electron J Biotechnol. 2000; 3:1995–2000. DOI: 10.2225/vol3-issue2-fulltext-5
14. Gilbert TW, Stolz DB, Biancaniello F, Simmons-Byrd A, Badylak SF. Production and characterization of ECM powder: implications for tissue engineering applications. Biomaterials. 2005; 26:1431–5. DOI: 10.1016/j.biomaterials.2004.04.042 [PubMed: 15482831]
15. Wise JB, Cabiling D, Yan D, Mirza N, Kirschner RE. Submucosal injection of micronized acellular dermal matrix: analysis of biocompatibility and durability. Plast Reconstr Surg. 2007; 120:1156–60. DOI: 10.1097/01.prs.0000279523.58632.0f [PubMed: 17898589]
16. Dreifuss SE, Wollstein R, Badylak SF, Rubin PJ. Acellular micronized extracellular matrix and occlusive dressings for open fingertip injuries. Plast Aesthetic Res. 2015; :2014–2015. DOI: 10.4103/2347-9264.156994
17. Sclafani A. Micronized acellular tissue for soft tissue augmentation. Aesthetic Surg J. 2000; 20:341–342. DOI: 10.1067/maj.2000.109063

18. Zuo H, Peng D, Zheng B, Liu X, Wang Y, Wang L, Zhou X, Liu J. Regeneration of mature dermis by transplanted particulate acellular dermal matrix in a rat model of skin defect wound. J Mater Sci Mater Med. 2012; 23:2933–44. DOI: 10.1007/s10856-012-4745-9 [PubMed: 22903602]

19. Freytes DO, Martin J, Velankar SS, Lee AS, Badylak SF. Preparation and rheological characterization of a gel form of the porcine urinary bladder matrix. Biomaterials. 2008; 29:1630–1637. DOI: 10.1016/j.biomaterials.2007.12.014 [PubMed: 18201760]

20. Singelyn JM, Dequach JA, Seif-naraghi SB, Littlefield RB, Schup-magoffin PJ, Christman KL. Naturally derived myocardial matrix as an injectable scaffold for cardiac tissue engineering. Biomaterials. 2009; 30:5409–5416. DOI: 10.1016/j.biomaterials.2009.06.045 [PubMed: 19608268]

21. Wolf MT, Daly KA, Brennan-Pierce EP, Johnson SA, Carruthers CA, D'Amore A, Nagarkar SP, Velankar SS, Badylak SF. A hydrogel derived from decellularized dermal extracellular matrix. Biomaterials. 2012; 33:7028–38. DOI: 10.1016/j.biomaterials.2012.06.051 [PubMed: 22789723]

22. Fu Y, Fan X, Tian C, Luo J, Zhang Y, Deng L, Qin T, Lv Q. Decellularization of porcine skeletal muscle extracellular matrix for the formulation of a matrix hydrogel: a preliminary study. J Cell Mol Med. 2016; :1–10. DOI: 10.1111/jcmm.12776

23. Tukmachev D, Forostyak S, Koci Z, Zaviskova K, Vackova I, Vyborny K, Sandvig I, Sandvig A, Medberry CJ, Badylak SF, Sykova E, Kubinova S. Injectable Extracellular Matrix Hydrogels as Scaffolds for Spinal Cord Injury Repair. Tissue Eng Part A. 2016; 22:306–17. DOI: 10.1089/ten.TEA.2015.0422 [PubMed: 26729284]

24. Sawkins MJ, Bowen W, Dhadda P, Markides H, Sidney LE, Taylor AJ, Rose FRAJ, Badylak SF, Shakesheff KM, White LJ. Hydrogels derived from demineralized and decellularized bone extracellular matrix. Acta Biomater. 2013; 9:7865–7873. DOI: 10.1016/j.actbio.2013.04.029 [PubMed: 23624219]

25. Medberry CJ, Crapo PM, Siu BF, Carruthers CA, Wolf MT, Nagarkar SP, Agrawal V, Jones KE, Kelly J, Johnson SA, Velankar SS, Watkins SC, Modo M, Badylak SF. Hydrogels derived from central nervous system extracellular matrix. Biomaterials. 2013; 34:1033–1040. DOI: 10.1016/j.biomaterials.2012.10.062 [PubMed: 23158935]

26. Seif-Naraghi SB, Singelyn JM, Salvatore MA, Osborn KG, Wang JJ, Sampat U, Kwan OL, Strachan GM, Wong J, Schup-Magoffin PJ, Braden RL, Bartels K, DeQuach JA, Preul M, Kinsey AM, DeMaria AN, Dib N, Christman KL. Safety and efficacy of an injectable extracellular matrix hydrogel for treating myocardial infarction. Sci Transl Med. 2013; 5:1–10. DOI: 10.1126/scitranslmed.3005503

27. O'Neill JD, Freytes DO, Anandappa AJ, Oliver JA, Vunjak-Novakovic GV. The regulation of growth and metabolism of kidney stem cells with regional specificity using extracellular matrix derived from kidney. Biomaterials. 2013; 34:9830–41. DOI: 10.1016/j.biomaterials.2013.09.022 [PubMed: 24074840]

28. Young DA, Ibrahim DO, Hu D, Christman KL. Injectable hydrogel scaffold from decellularized human lipoaspirate. Acta Biomater. 2011; 7:1040–1049. DOI: 10.1016/j.actbio.2010.09.035 [PubMed: 20932943]

29. Burnsed OA, Schwartz Z, Marchand KO, Hyzy SL, Olivares-Navarrete R, Boyan BD. Hydrogels Derived from Cartilage Matrices Promote Induction of Human Mesenchymal Stem Cell Chondrogenic Differentiation. Acta Biomater. 2016; doi: 10.1016/j.actbio.2016.07.034

30. Bergmeister H, Boeck P, Kasimir M, Fleck T, Fitzal F, Husinsky W, Mittlboeck M, Stoehr HG, Losert U, Wolner E, Grabenwoeger M. Effect of Laser Perforation on the Remodeling of Acellular Matrix Grafts. J Biomed Mater Res Part B. 2005; :495–503. DOI: 10.1002/jbm.b.30228

31. Kasyanov VA, Hodde J, Hiles MC, Eisenberg C, Eisenberg L, De Castro LEF, Ozolanta I, Murovska M, Draughn RA, Prestwich GD, Markwald RR, Mironov V. Rapid biofabrication of tubular tissue constructs by centrifugal casting in a decellularized natural scaffold with laser-machined micropores. J Mater Sci Mater Med. 2009; :329–337. DOI: 10.1007/s10856-008-3590-3

32. Sheridan WS, Duffy GP, Murphy BP. Mechanical characterization of a customized decellularized scaffold for vascular tissue engineering. J Mech Behav Biomed Mater. 2012; 8:58–70. DOI: 10.1016/j.jmbbm.2011.12.003 [PubMed: 22402154]

33. Xu H, Wan H, Zuo W, Sun W, Owens RT, Harper JR, Ayares DL, McQuillan DJ. A porcine-derived acellular dermal scaffold that supports soft tissue regeneration: removal of terminal

galactose-alpha-(1,3)-galactose and retention of matrix structure. Tissue Eng Part A. 2009; 15:1807–1819. DOI: 10.1089/ten.tea.2008.0384 [PubMed: 19196142]

34. Stone KR, Walgenbach A, Galili U. Induced Remodeling of Porcine Tendons to Human Anterior Cruciate Ligaments by a -GAL Epitope Removal and Partial Cross-Linking. Tissue Eng Part B. 2017; 23:412–419. DOI: 10.1089/ten.teb.2016.0332
35. Gao H, Li S, Sun WQ, Yun Z, Zhang X, Song J, Zhang S, Leng L, Ji S, Tan Y, Gong F. Quantification of a -Gal Antigen Removal in the Porcine Dermal Tissue by a -Galactosidase. Tissue Eng Part C. 2015; 21:1197–1204. DOI: 10.1089/ten.tec.2015.0129
36. Lu Q, Ganesan K, Simionescu DT, Vyavahare NR. Novel porous aortic elastin and collagen scaffolds for tissue engineering. Biomaterials. 2004; 25:5227–5237. DOI: 10.1016/j.biomaterials.2003.12.019 [PubMed: 15110474]
37. Boer U, Spengler C, Jonigk D, Klingenberg M, Schrimpf C, Lu S, Harder M, Kreipe H, Haverich A, Wilhelmi M. Coating Decellularized Equine Carotid Arteries with CCN1 Improves Cellular Repopulation, Local Biocompatibility. Tissue Eng Part A. 2013; 19doi: 10.1089/ten.tea.2012.0558
38. Evren S, Loai Y, Antoon R, Islam S, Yeger H, Moore K, Wong K, Gorczynski R, Farhat WA. Urinary bladder tissue engineering using natural scaffolds in a porcine model: Role of toll-like receptors and impact of biomimetic molecules. Cells Tissues Organs. 2010; 192:250–261. DOI: 10.1159/000317332 [PubMed: 20588005]
39. Koobatian MT, Row S, Smith RJ, Koenigsknecht C, Andreadis ST, Swartz DD. Successful endothelialization and remodeling of a cell-free small-diameter arterial graft in a large animal model. Biomaterials. 2016; 76:344–358. DOI: 10.1016/j.biomaterials.2015.10.020 [PubMed: 26561932]
40. De Cock LJ, De Koker S, De Vos F, Vervaet C, Remon JP, De Geest BG. Layer-by-layer incorporation of growth factors in decellularized aortic heart valve leaflets. Biomacromolecules. 2010; 11:1002–1008. DOI: 10.1021/bm9014649 [PubMed: 20155947]
41. Fitzpatrick LE, McDevitt TC. Cell-derived matrices for tissue engineering and regenerative medicine applications. Biomater Sci. 2014; doi: 10.1039/C4BM00246F
42. Papadimitropoulos A, Scotti C, Bourgine P, Scherberich A, Martin I. Engineered decellularized matrices to instruct bone regeneration processes. Bone. 2014; doi: 10.1016/j.bone.2014.09.007
43. Bourgine PE, Pippenger BE, Todorov A, Tchang L, Martin I. Tissue decellularization by activation of programmed cell death. Biomaterials. 2013; 34:6099–108. DOI: 10.1016/j.biomaterials.2013.04.058 [PubMed: 23721795]
44. Bourgine PE, Gaudiello E, Pippenger B, Jaquiery C, Klein T, Pigeot S, Todorov A, Feliciano S, Banfi A, Martin I. Engineered Extracellular Matrices as Biomaterials of Tunable Composition and Function. Adv Funct Mater. 2017; :1605486.doi: 10.1002/adfm.201605486
45. Kyriakides TR, Zhu YH, Smith LT, Bain SD, Yang Z, Lin MT, Danielson KG, Iozzo RV, LaMarca M, McKinney CE, Ginns EI, Bornstein P. Mice that lack thrombospondin 2 display connective tissue abnormalities that are associated with disordered collagen fibrillogenesis, an increased vascular density, and a bleeding diathesis. J Cell Biol. 1998; 140:419–30. [PubMed: 9442117]
46. Krady MM, Zeng J, Yu J, MacLauchlan S, Skokos EA, Tian W, Bornstein P, Sessa WC, Kyriakides TR. Thrombospondin-2 modulates extracellular matrix remodeling during physiological angiogenesis. Am J Pathol. 2008; 173:879–91. DOI: 10.2353/ajpath.2008.080128 [PubMed: 18688033]
47. Calabro NE, Kristofik NJ, Kyriakides TR. Thrombospondin-2 and extracellular matrix assembly. Biochim Biophys Acta. 2014; 1840:2396–2402. DOI: 10.1016/j.bbagen.2014.01.013 [PubMed: 24440155]
48. Kyriakides TR, Maclauchlan S. The role of thrombospondins in wound healing, ischemia, and the foreign body reaction. J Cell Commun Signal. 2009; 3:215–25. DOI: 10.1007/s12079-009-0077-z [PubMed: 19844806]
49. Kristofik N, Calabro NE, Tian W, Meng A, MacLauchlan S, Wang Y, Breuer CK, Tellides G, Niklason LE, Kyriakides TR. Impaired von Willebrand factor adhesion and platelet response in thrombospondin-2 knockout mice. Blood. 2016; doi: 10.1182/blood-2016-03-702845

50. Kristofik NJ, Qin L, Calabro NE, Dimitrievska S, Li G, Tellides G, Niklason LE, Kyriakides TR. Improving in vivo outcomes of decellularized vascular grafts via incorporation of a novel extracellular matrix. Biomaterials. 2017; 141:63–73. [PubMed: 28667900]
51. Hwang J, Hoa B, Turner NJ, White LJ, Faulk DM, Badylak SF, Li Y, Yu SM. Molecular assessment of collagen denaturation in decellularized tissues using a collagen hybridizing peptide. Acta Biomater. 2017; 53:268–278. DOI: 10.1016/j.actbio.2017.01.079 [PubMed: 28161576]
52. Reing JE, Zhang L, Myers-Irvin J, Cordero KE, Freytes DO, Heber-Katz E, Bedelbaeva K, McIntosh D, Dewilde A, Braunhut SJ, Badylak SF. Degradation products of extracellular matrix affect cell migration and proliferation. Tissue Eng Part A. 2009; 15:605–14. DOI: 10.1089/ten.tea.2007.0425 [PubMed: 18652541]
53. Dearth CL, Keane TJ, Scott JR, Daly KA, Badylak SF. A Rodent Model to Evaluate the Tissue Response to a Biological Scaffold When Adjacent to a Synthetic Material. Tissue Eng Part A. 2015; 21:2526–2535. DOI: 10.1089/ten.tea.2014.0649 [PubMed: 26176992]
54. Morris AH, Mahal RS, Udell J, Wu M, Kyriakides TR. Multicompartment Drug Release System for Dynamic Modulation of Tissue Responses. Adv Healthc Mater. 2017; 1700370:1700370.doi: 10.1002/adhm.201700370
55. Kyriakides TR, Leach KJ, Hoffman AS, Ratner BD, Bornstein P. Mice that lack the angiogenesis inhibitor, thrombospondin 2, mount an altered foreign body reaction characterized by increased vascularity. Proc Natl Acad Sci U S A. 1999; 96:4449–54. http://www.pubmedcentral.nih.gov/articlerender.fcgi?artid=16352&tool=pmcentrez&rendertype=abstract. [PubMed: 10200282]
56. Kyriakides TR, Tam JWY, Bornstein P. Accelerated Wound Healing in Mice With a Disruption of the Thrombospondin 2 Gene. J Invest Dermatol. 1999; 113:782–787. [PubMed: 10571734]
57. Kobsa S, Kristofik NJ, Sawyer AJ, Bothwell ALM, Kyriakides TR, Saltzman WM. An electrospun scaffold integrating nucleic acid delivery for treatment of full-thickness wounds. Biomaterials. 2013; 34:3891–901. DOI: 10.1016/j.biomaterials.2013.02.016 [PubMed: 23453058]
58. Moyer HR, Hart AM, Yeager J, Losken A. A Histological Comparison of Two Human Acellular Dermal Matrix Products in Prosthetic-Based Breast Reconstruction. Plast Reconstr Surg – Glob Open. 2017; 5:e1576.doi: 10.1097/GOX.0000000000001576 [PubMed: 29632762]
59. Margolis DJ, Malay DS, Hoffstad OJ, Leonard CE, MaCurdy T, Nava KL de, Tan Y, Molina T, Siegel KL. Incidence of diabetic foot ulcer and lower extremity amputation among Medicare beneficiaries, 2006 to 2008, in. Data Points #2. 2011
60. Margolis DJ, Malay DS, Hoffstad OJ, Leonard CE, MaCurdy T, Nava KL de, Tan Y, Molina T, Siegel KL. Prevalence of diabetes, diabetic foot ulcer, and lower extremity amputation among Medicare beneficiaries, 2006 to 2008, in. Data Points #1. 2011
61. Weledji EP, Fokam P. Treatment of the diabetic foot – to amputate or not? BMC Surg. 2014; 14:1–6. [PubMed: 24401085]

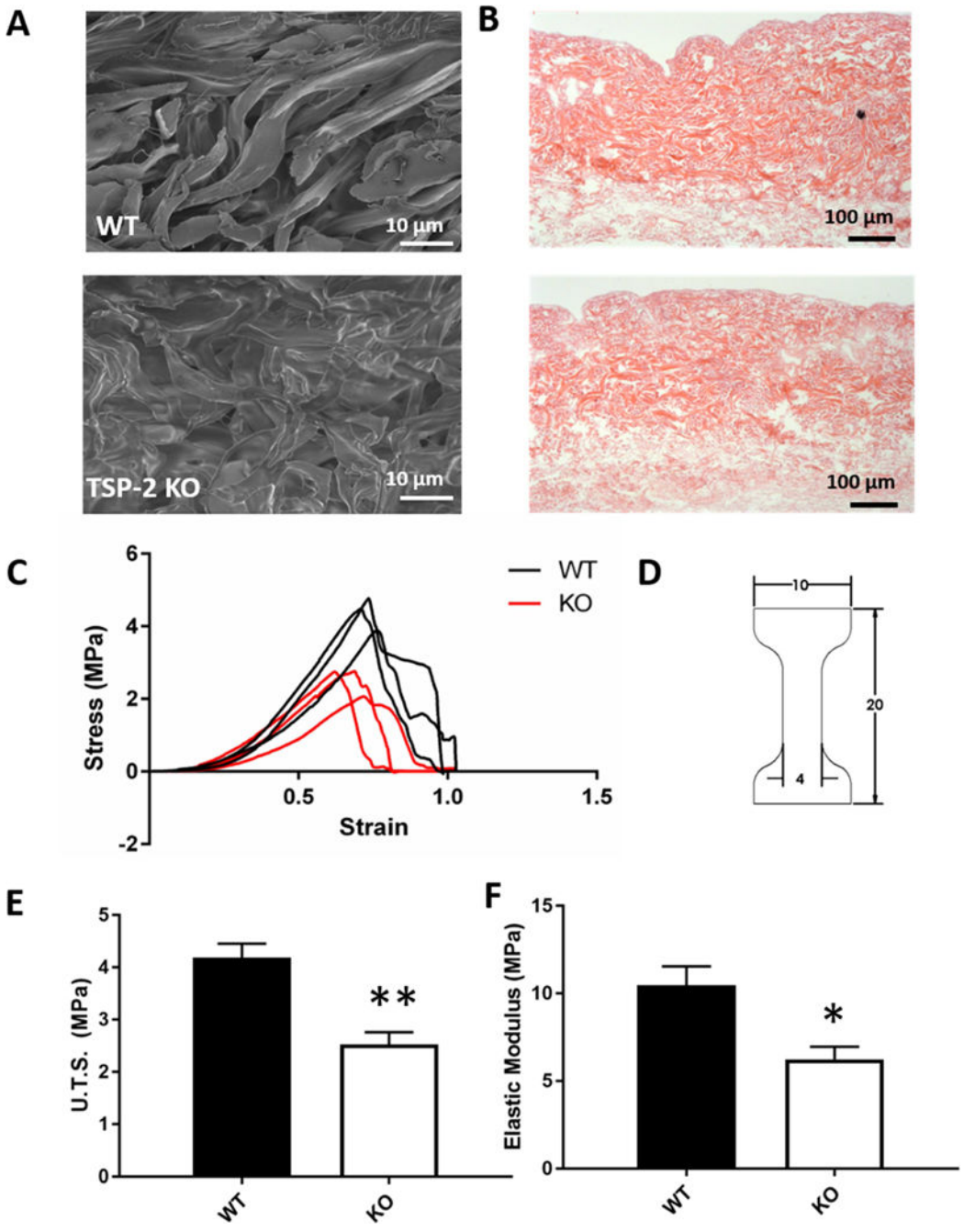

Fig. 1. TSP-2 KO ADM exhibits altered structure and mechanics

Representative SEM demonstrating contrast between structures (A). Representative H&E images indicating the absence of nuclear material in both constructs (B). Stress versus strain plots of tensile testing (C) and diagram of dog bone-shaped cutouts (units in mm) (D). Ultimate tensile strength (E) and elastic modulus (F) of WT and TSP-2 KO constructs. Results are given as mean + SEM, n=3, *p<0.05, **p<0.01.

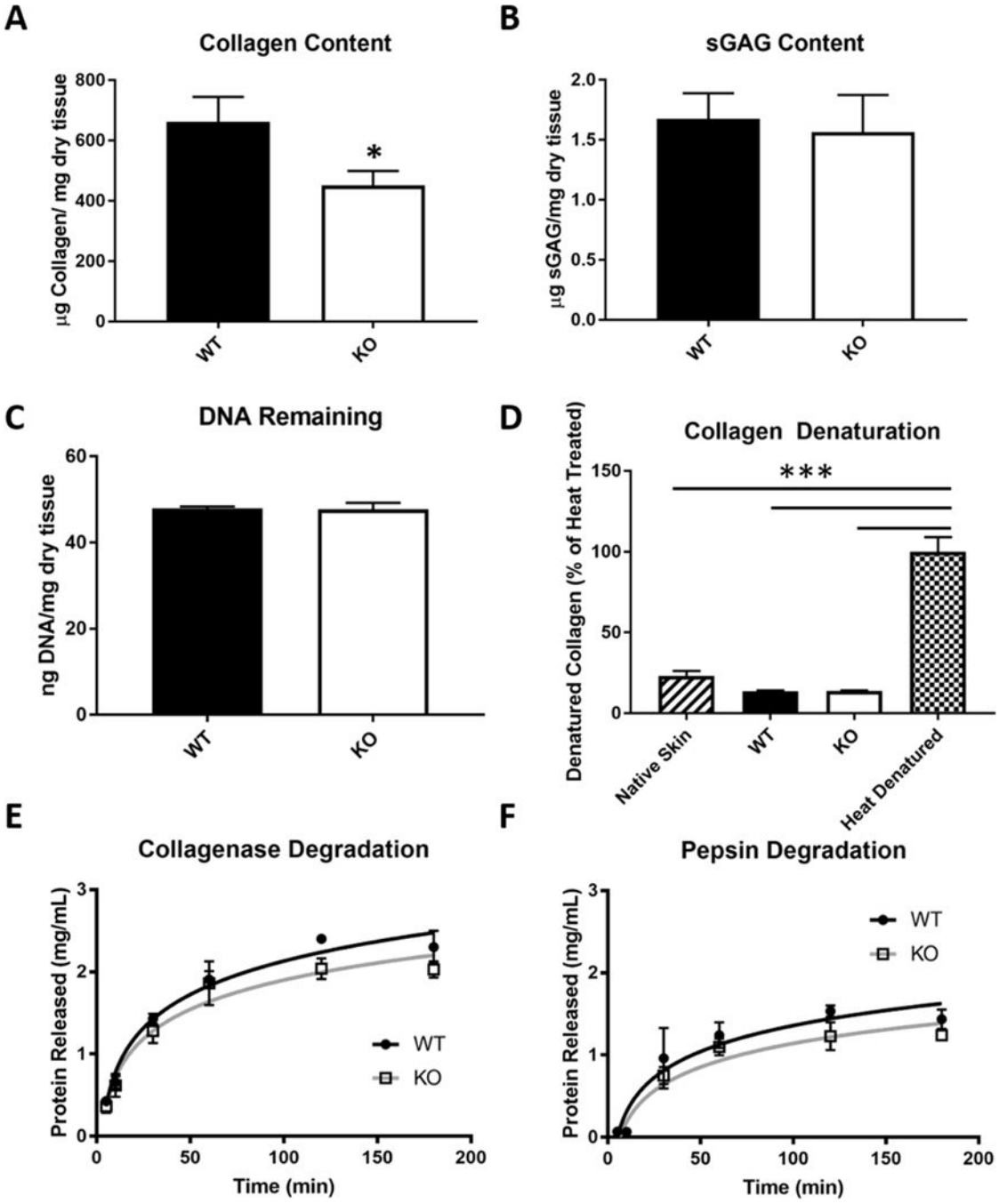

Fig. 2. TSP-2 KO ADM exhibits reduced collagen content, but is otherwise biochemically similar

TSP-2 KO decellularized skin constructs exhibited reduced collagen content as compared to WT by hydroxyproline assay (n=7) (A). sGAG content (B) and residual DNA (C) were unchanged between genotypes (n=3). There was no difference in denaturation between WT and TSP-2 KO constructs compared to native skin. Each of these three exhibited significantly less denaturation than heat-denatured native skin (n=3) (D). Enzymatic degradation kinetics demonstrate no difference in susceptibility between WT and TSP-2 KO

constructs to either collagenase (E) or pepsin (F) (n=3). Results are given as mean + SEM, *p<0.05, ***p<0.0001.

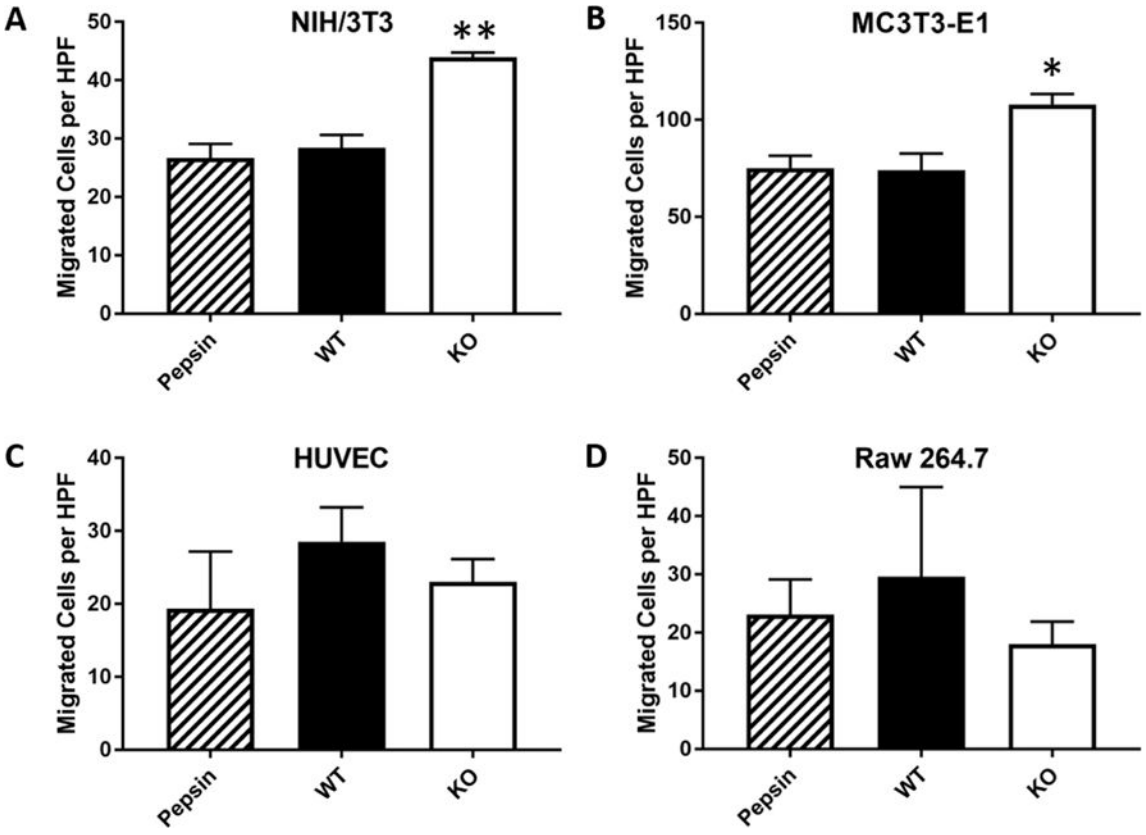

Fig. 3. TSP-2 KO degradation products induce chemotactic effects

Degradation products were prepared by incubating decellularized skin in a pepsin solution. Degradation products were added to serum-free media at a concentration of 50 μg/mL, and chemotaxis toward them was tested in a Transwell. NIH/3T3 embryonic fibroblasts (A) and MC3T3-E1 preosteoblasts (B) migration significantly increased toward TSP-2 KO matrix than the pepsin control. WT display no greater chemotaxis than control. HUVECs (C) and RAW 264.7 macrophages (D) display no chemotactic activity toward either degradation product (n=3).

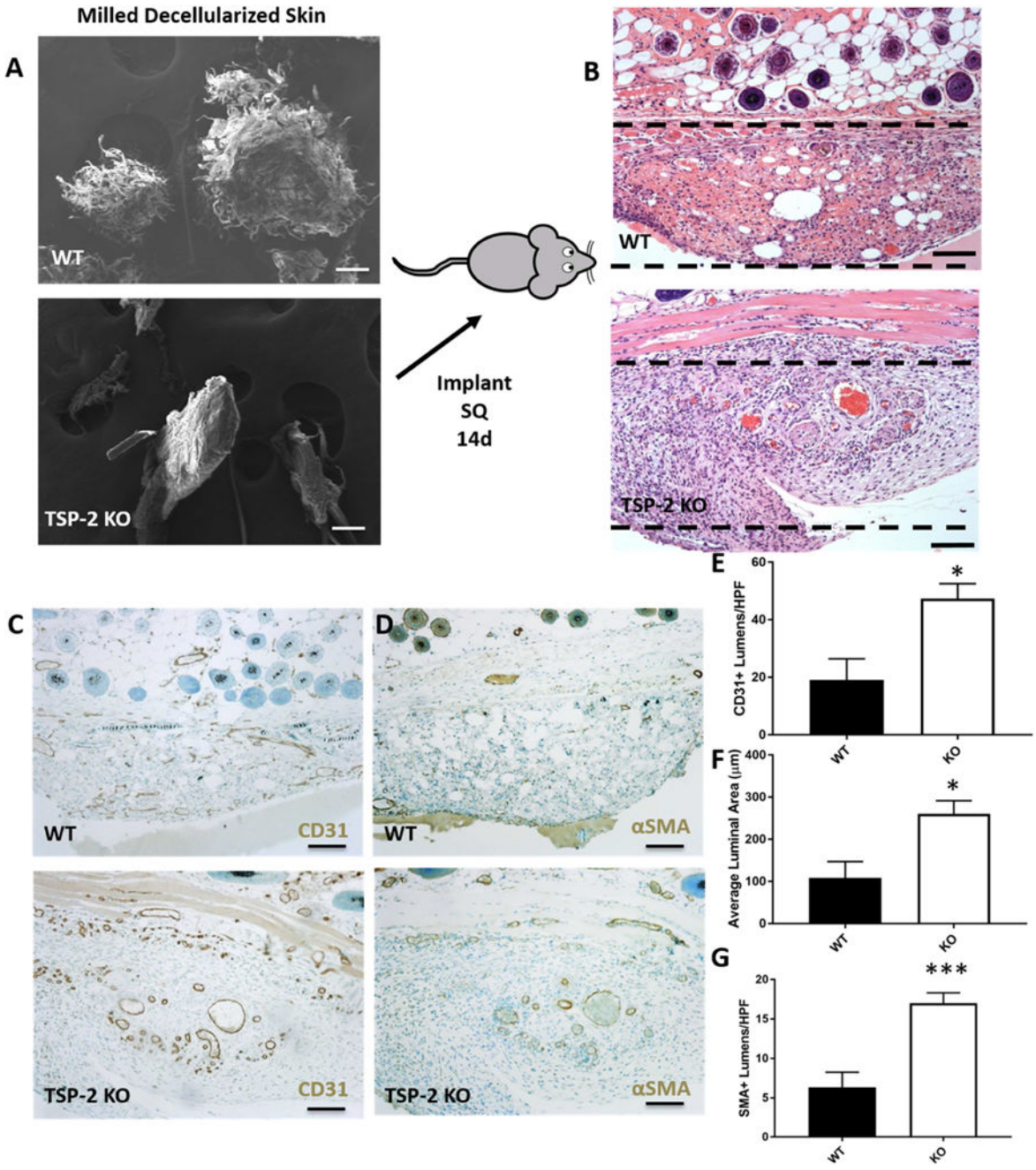

Fig. 4. Comminuted TSP-2 KO ADM promotes vascularization

SEM of WT and TSP-2 KO powdered ECM indicated difference in the structure of the grains, with WT appearing more shredded (A). After 14 days *in vivo* the powder was well invaded (B). Immunohistochemistry demonstrated more vascularization around the TSP-2 KO powder as demonstrated by CD31 (C) and αSMA (D). There were more CD31-positive lumens (E) that were larger (F) and more αSMA-positive (G). Scale bars = 100 μm. Implanted silicone trays are out of frame but reside below and to the sides of the implanted ECM. ECM is just below the dermis. Results are given as mean + SEM, n=6, *p<0.05, ***p<0.005.

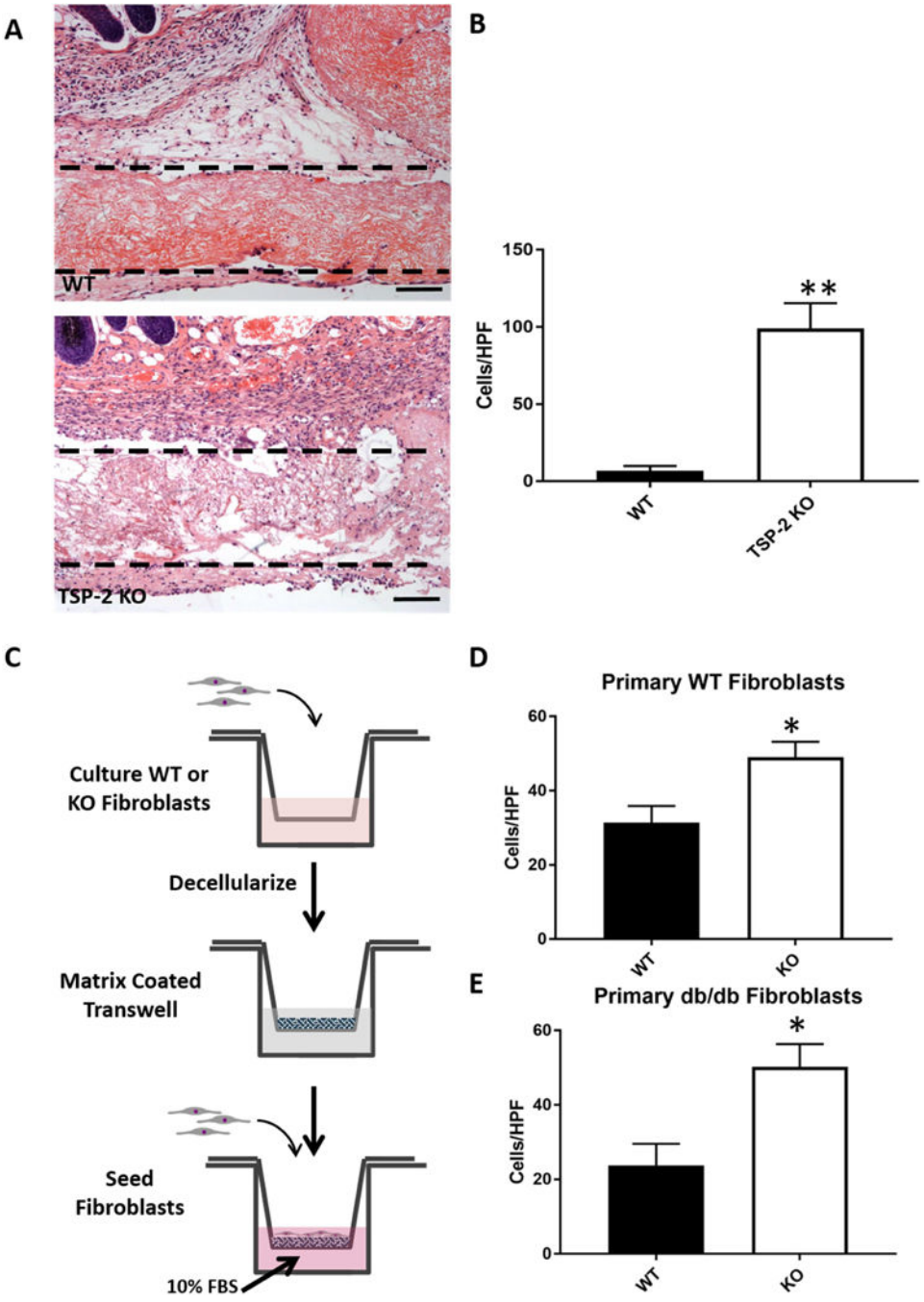

Fig. 5. TSP-2 KO matrix promotes a pro-migratory environment

Intact slabs of constructs were implanted subcutaneously for 14 days, scale bar = 100 μm (A), and TSP-2 KO constructs display increased cell penetration into the matrix. Implanted silicone trays are out of frame but reside below and to the sides of the implanted ECM; ECM is just below the dermis (n=4) (B). CDM was analyzed as an *in vitro* system to probe cell migration through WT and TSP-2 KO matrix (C), and it was found that TSP-2 null ECM is more permissive to both WT and db/db fibroblast migration, n=5 (D–E). Scale bars = 100 μm. Results are given as mean + SEM, *p<0.05, **p<0.01.

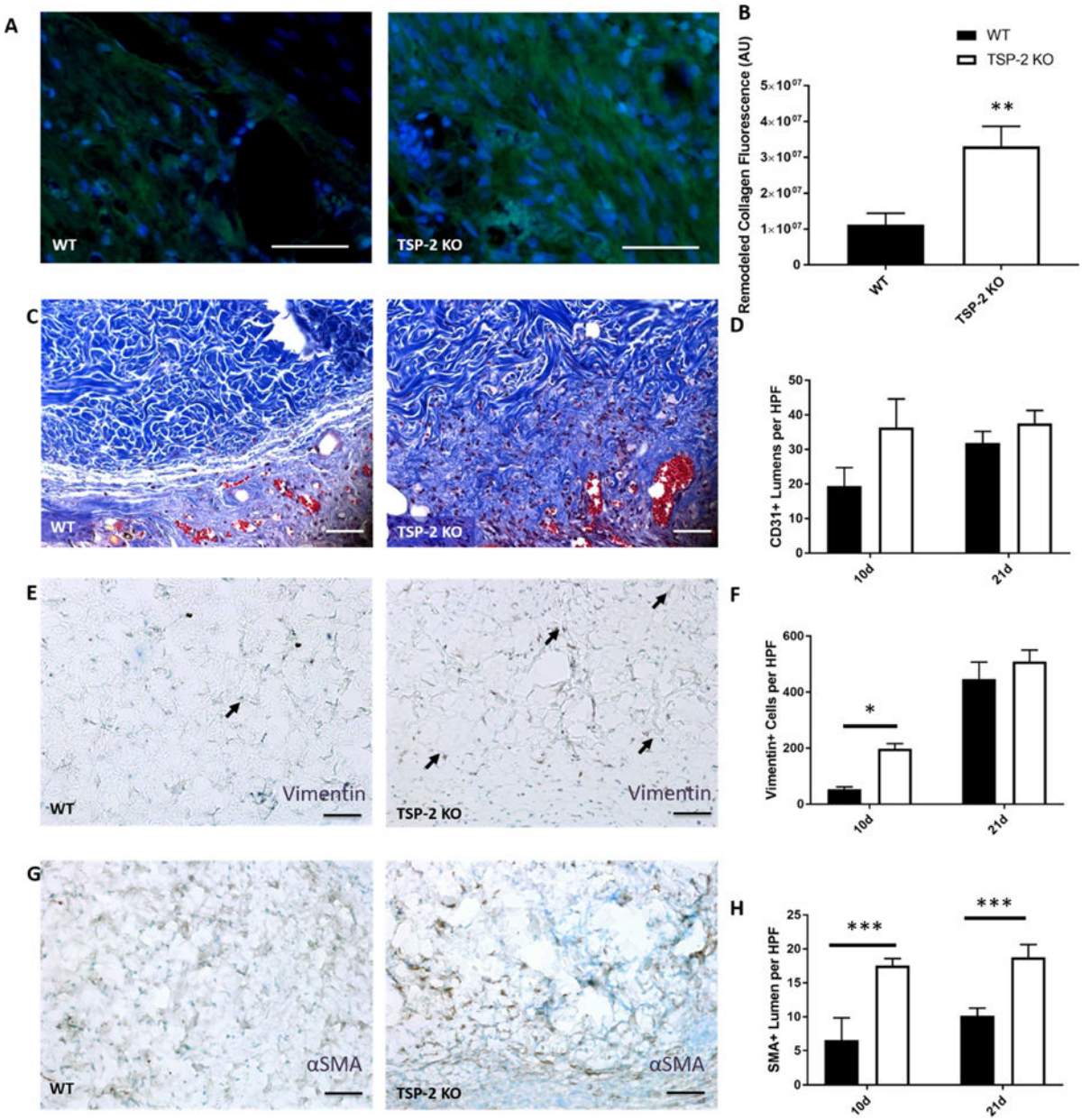

Fig. 6. TSP-2 KO ADM exhibits enhanced integration and vascular maturation in diabetic wounds

Representative images of collagen remodeling in ADM after 10 days of implantation in diabetic wounds (A) demonstrate increased remodeling in TSP-2 KO ADM (B). Representative images of Masson's trichrome staining along border of graft demonstrate increased tissue integration with TSP-2 KO ADM; the border between normal tissue and graft is no longer visible by 10 days (C). There are no differences in total vessel number (CD31) between WT and TSP-2 KO ADM treated wounds at 10 or 21 days (D). Representative images of vimentin staining after 10 days (E). Quantification of vimentin stain indicates an increased penetration of mesenchymal cells within the TSP-2 KO ADM by 10 days, but the WT ADM were no different by 21 days (F). Representative images of

αSMA after 10 days (G) and quantification revealing more positive vessels at both 10 and 21 days. n=4 (10 days) or n=6 (21 days). Scale bars = 50 μm. Results are given as mean + SEM, *p<0.05, **p<0.01.